



Showcasing research from Professor Ken-ichi Sakai's laboratory,  
Chitose Institute of Science and Technology, Chitose, Japan.

Harnessing inhomogeneous  $\pi$ -aggregates: a new path to optical modulation in methyl salicylate-based solvent-free liquids

When an alkoxy chain with a carbon number of four to seven is introduced at the 5-position of methyl salicylate (MS), the originally colourless liquid turns vivid yellow and exhibits distinct absorption and fluorescence spectra. The emergence of these optical properties indicates that alkoxylation promotes the formation of unique  $\pi$ -aggregates in the liquid phase. Within these locally ordered aggregates,  $\pi$ -electrons appear to be delocalized over multiple MS molecules, giving rise to collective electronic interactions responsible for the characteristic colour and fluorescence behaviour.

Image reproduced by permission of Ken-ichi Sakai from *Chem. Sci.*, 2025, **16**, 21797.

## As featured in:



See Ken-ichi Sakai *et al.*,  
*Chem. Sci.*, 2025, **16**, 21797.



Cite this: *Chem. Sci.*, 2025, **16**, 21797

All publication charges for this article have been paid for by the Royal Society of Chemistry

## Harnessing inhomogeneous $\pi$ -aggregates: a new path to optical modulation in methyl salicylate-based solvent-free liquids

Kei Kobayashi, <sup>a</sup> Ken-ichi Sakai, <sup>\*a</sup> Tomoyuki Akutagawa <sup>b</sup> and Takashi Nakanishi <sup>c</sup>

Liquids are characterized by macroscopic isotropy and homogeneity, yet they can exhibit the ability to self-organize at the molecular level. Driven by intermolecular forces such as coulombic and dispersion interactions, the constituent molecules spontaneously form locally heterogeneous structures. This behavior highlights the dynamic complexity and inherent adaptability of liquid systems. We found that methyl salicylate (MS), a colourless liquid, transforms into a vivid yellow liquid with distinct absorption and fluorescence spectral characteristics when an alkoxy chain with a carbon number of four to seven is attached to the 5-position of MS. This phenomenon suggests the presence of microscopic local structures in the liquids, where  $\pi$ -electrons are delocalized across multiple MS molecules. X-ray diffraction (XRD) measurements supported this interpretation by indicating aggregates in the 10–15 Å range, composed of about three to five MS molecules arranged in a face-to-face  $\pi$ -stacking configuration. When the alkylated MS liquids are heated from temperatures below their glass transition temperature, they exhibit the property of crystallizing from a supercooled liquid state, known as cold crystallization. Furthermore, free-volume analysis using positron annihilation lifetime spectroscopy (PALS) suggested that the yellow liquids have fewer free-volume regions compared to the unsubstituted MS colourless liquid. Consistent with these findings, time-resolved fluorescence spectroscopy of the neat yellow liquids revealed a relatively longer lifetime of 20 ns, which is likely attributable to fluorescence from  $\pi$ -aggregates, distinct from the 0.5 ns shorter lifetime component observed for single molecules in diluted solutions. All of these results support the presence of  $\pi$ -aggregates, which contribute to the colour and fluorescence of the liquids. Supramolecular aggregates in liquids have been studied both experimentally and theoretically; however, the alkylated MS liquids represent the first example in which they significantly affect the optical properties of the liquids.

Received 13th August 2025  
Accepted 21st October 2025

DOI: 10.1039/d5sc06148b  
[rsc.li/chemical-science](http://rsc.li/chemical-science)

## Introduction

In condensed systems of  $\pi$ -electronic molecules, the arrangement of the molecules is closely related to the functionalities they offer; particularly, the carrier transport properties are significantly influenced by intermolecular interactions, such as vertical  $\pi$ – $\pi$  overlaps and side-by-side sulfur–sulfur contacts.<sup>1</sup> Peripheral modification of  $\pi$ -molecules with linear alkyl chains is an effective strategy for controlling molecular arrangement. This approach can enhance intermolecular interactions, contributing not only to the development of high-performance organic devices and their facile fabrication,<sup>2,3</sup> but also to the

design of liquid crystal molecules, especially by improving alignment properties and stabilizing the liquid crystal phase.<sup>4</sup> Meanwhile, such modifications contribute to increasing solubility of  $\pi$ -molecules to solvents, thereby facilitating better processability using solution processing methods. Although bulkier modifications, such as the use of branched alkyl chains, can rather act as obstacles to intermolecular  $\pi$ – $\pi$  interactions, they can also offer a new category of materials called molecular liquids, which are anticipated to have promising uses for soft electronics.<sup>5–9</sup>

On the other hand, it is rather challenging to derive optical properties from condensed systems of  $\pi$ -molecules. Regarding fluorescence properties, intermolecular interactions tend to cause fluorescence quenching, and in fact, examples of organic crystals showing high fluorescence are limited.<sup>10</sup> Aggregate-induced emission enhancement (AIEE) is a phenomenon that addresses this quenching problem,<sup>11</sup> but the emission does not come from molecular aggregates; rather, it comes from individual molecules whose intramolecular motions are restricted

<sup>a</sup>Graduate School of Science and Technology, Chitose Institute of Science and Technology (CIST), Chitose 066-8655, Japan. E-mail: [k-sakai@photon.chitose.ac.jp](mailto:k-sakai@photon.chitose.ac.jp)

<sup>b</sup>Polymer Hybrid Materials Research Center, Institute of Multidisciplinary Research for Advanced Materials (IMRAM), Tohoku University, Sendai 980-8577, Japan

<sup>c</sup>Research Center for Materials Nanoarchitectonics (MANA), National Institute for Materials Science (NIMS), 1-1 Namiki, Tsukuba 305-0044, Japan



by aggregation. Thus, fluorescence from excited states involving multiple  $\pi$ -molecules is uncommon. An exception is fluorescence from J-aggregates composed of head-to-tail molecular arrangements, which results from intermolecular exciton coupling among multiple  $\pi$ -molecules.<sup>12</sup> Such J-aggregates exhibit unique absorption and fluorescence spectra, showing bathochromic shifts, sharpened linewidths, and much smaller Stokes shifts compared to those of individual chromophores. Introduction of linear alkyl/alkoxy chains to chromophores can be effective to construct J-aggregates.<sup>13</sup> To the best of our knowledge, no other examples of aggregate-based fluorescence like that seen in J-aggregates have been reported. However, we recently found that small  $\pi$ -molecules such as methyl salicylate (MS) dyad-type molecules<sup>14</sup> and octahydro-binaphthols<sup>15</sup> exhibit characteristic fluorescence bands in the longer-wavelength region with increasing concentration, reaching maximum intensities at significantly higher concentrations (around 0.1 M) than those at which typical fluorescent chromophores exhibit quenching. Actually, such small aromatic molecules are not expected to have effective  $\pi$ - $\pi$  interaction,<sup>16–18</sup> but we concluded that these fluorescence bands originate from  $\pi$ -slipped stacked aggregates formed under high concentration conditions, where intermolecular orbital mixing is compatible, resulting in delocalization of  $\pi$ -electrons over multiple molecules.

Alkyl- $\pi$  molecular liquids are also attracting interest as photofunctional materials,<sup>19–29</sup> in which it is important to construct a concentrated system that maximizes the number of chromophores without degrading their luminescent properties.<sup>30</sup> In the ongoing research on MS derivatives, we obtained highly-fluorescent molecular liquids by linking a linear alkoxy chain to MS (Fig. 1a), whose unique colour appearance and fluorescence properties cannot be explained as those of the MS molecules themselves. This suggests that microscopic local MS aggregates with  $\pi$ -slipped stacked structures exist within a homogeneous liquid state. Although it depends on the

timescale of observation, liquids are generally isotropic and homogeneous on a macroscopic scale. Nevertheless, they often exhibit molecular-level inhomogeneity due to the formation of aggregates when effective intermolecular interactions are present.<sup>31–34</sup> In particular, ionic liquids, governed by relatively strong coulombic interactions, are known to be nano-heterogeneous yet coherent and essentially regular liquids that exhibit nanoscale structural organization.<sup>35</sup> Studies aiming to utilize such heterogeneity to induce the functionality of molecular liquids have been conducted, for example, on dynamic aggregates in alkyl-pyrene liquids, which give rise to excimer formation and influence liquid viscosity,<sup>36,37</sup> and on insoluble aggregates formed in liquid–liquid blends that enable luminescent colour tuning.<sup>38</sup> However, there have been only limited reports directly attributing the optical properties (colour and fluorescence) of molecular liquids to such multi-molecular aggregates as introduced in this study. Here, we argue that the alkoxy-chain-linked MS liquids represent a novel class of molecular liquid by confirming the validity of our interpretation.

## Results and discussion

### Optical properties of MS derivatives with varying alkoxy chain lengths

Both MS and methyl 5-methoxysalicylate (**1**) are colourless liquids, whereas the other synthesized samples were obtained in the following states depending on the length of the alkoxy chain (Fig. 1b, upper row): **2** and **3** were light yellow powders, **4**, **5**, **6**, and **7** were highlighter yellow liquids, and **8**, **9**, and **10** were yellow powders. Although the absorption band edges of the colourless liquids (MS and **1**) lie in the UV region, approximately below 400 nm (Fig. 1c, dotted red and blue lines, respectively), yellow liquids (**4**–**7**) exhibit characteristic absorption bands with fine vibronic progressions in the region of 400–500 nm (dotted green line for **5** in Fig. 1c). Similar features are also detectable when **2** or **3** are dissolved in solution at a high concentration of around 0.1 M (Fig. S1, SI). These spectral characteristics are almost the same as those observed for MS-dyads in high-concentration solutions, for which we have previously concluded that linking two MS units makes it possible to form stable aggregates with a  $\pi$ -stacking of MS moieties, resulting in their appearance.<sup>14</sup> In this study, however, we revise our previous understanding and conclude that the stabilization of MS aggregates is achieved simply by linking alkoxy chains with two or more carbon atoms. Since all samples—including **1** to **3** as well as **4** to **10**—formed colourless solutions upon dilution with solvent, giving an identical absorption spectrum with a maximum at 340 nm (Fig. S2, SI), stable  $\pi$ -aggregates appear to form only under condensed conditions, such as neat liquids (**4**–**7**) and highly concentrated solutions over  $10^{-1}$  M (**2**, **3**, **8**–**10**).

With regard to fluorescence, both MS and **1**, despite being colourless, exhibit bands in the relatively long-wavelength region of 400–600 nm (Fig. 1c, solid red and blue lines, respectively). These behaviours are due to their undergoing excited-state intramolecular proton transfer (ESIPT), which results in a large Stokes shift.<sup>39,40</sup> In contrast to the blue

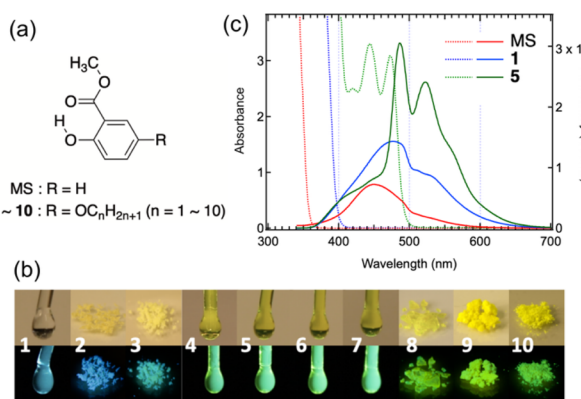


Fig. 1 (a) Chemical structures of methyl salicylate (MS) and methyl 5-alkoxysalicylates (1–10). (b) Photographs of 1–10 taken under white light (top) and 365 nm UV light (bottom). (c) Absorption (dotted lines) and fluorescence (solid lines) spectra of neat liquid MS (red), **1** (blue), and **5** (green), measured using a 1 mm path length cell. The excitation wavelength ( $\lambda_{\text{ex}}$ ) was 330 nm. Fluorescence spectra of the other samples are presented in Fig. S3, SI.



fluorescence of MS and **1**, all of the yellow liquids (**4–7**) exhibit light green fluorescence (Fig. 1b, lower row), whose spectra are nearly mirror images of their absorption spectra (solid green line for **5** in Fig. 1c). Even in the colourless liquid (**1**), however, a faint trace of this characteristic fluorescence band can be detected, when excited at 470 nm, despite the absence of absorption at that wavelength.<sup>14</sup> In fact, when the yellow liquids (**4–7**) are sandwiched between quartz plates, they appear colourless and show no absorption in the visible region, but the characteristic fluorescence band can still be clearly observed (Fig. S4, SI). Overall, the results indicate that fluorescence spectroscopy provides a more sensitive means of detecting  $\pi$ -aggregates even in colourless liquids, where absorption spectroscopy yields little information, and that the  $\pi$ -aggregates formed in **4–7** are significantly more stable than those in **1**, thereby enabling the clear expression of the characteristic absorption and fluorescence spectra.

The aggregates in the MS-liquid are considered to be passively formed as a result of molecular crowding in the highly concentrated liquid phase, in contrast to self-assembling J-aggregates of molecules possessing large association constants in solution. In practice, upon heating, no change in the spectral shape suggestive of aggregate dissociation was observed, while a decrease in intensity attributable to thermal deactivation was detected (Fig. S5, SI).

### Crystallization behaviour and thermal properties of MS liquids

To assess the thermal phase transitions of the MS liquids, differential scanning calorimetry (DSC) measurements were performed at a rate of  $10\text{ }^{\circ}\text{C min}^{-1}$  (Fig. 2a: liquid sample results; Fig. S6, SI: powder sample results; Table S1, SI: thermal data for all samples; Fig. 2b: visual representation corresponding to Table S1). Although it was hard to discern signals in the cooling traces down to  $-100\text{ }^{\circ}\text{C}$  for each of the liquid samples (**1**, **4–7**), very weak exothermic peaks were detected around  $-42\text{ }^{\circ}\text{C}$  to  $-46\text{ }^{\circ}\text{C}$  (orange squares with dotted outlines in Fig. 2a). On the other hand, in the subsequent heating traces, all samples exhibited very weak endothermic features, likely associated with the glass transition ( $T_g$ ) occurring between  $-74\text{ }^{\circ}\text{C}$  and  $-64\text{ }^{\circ}\text{C}$  (green squares with dotted outlines in Fig. 2a), followed by distinct exothermic crystallization peaks and endothermic melting ( $T_m$ ) peaks, except for **4**, which exhibited a broad rise with a crystallization peak at  $-0.7\text{ }^{\circ}\text{C}$ . These crystallization peaks during the heating process are attributed to crystallization from the supercooled liquid or glassy state, a phenomenon known as cold crystallization (CC). In general, CC refers to the process in which polymers, initially transformed into a glass state by cooling, undergo crystallization upon heating.<sup>41</sup> However, CC has increasingly been observed even in small molecules.<sup>25,42–46</sup> In the case of small molecules, glass formation, supercooling, and crystallization compete with one another, influenced by factors such as diffusion and crystallization rates, molecular geometry and flexibility and intermolecular interactions; in fact, the rapid glass-to-crystal (GC) transition occurring near  $T_g$  of fragile liquids has been

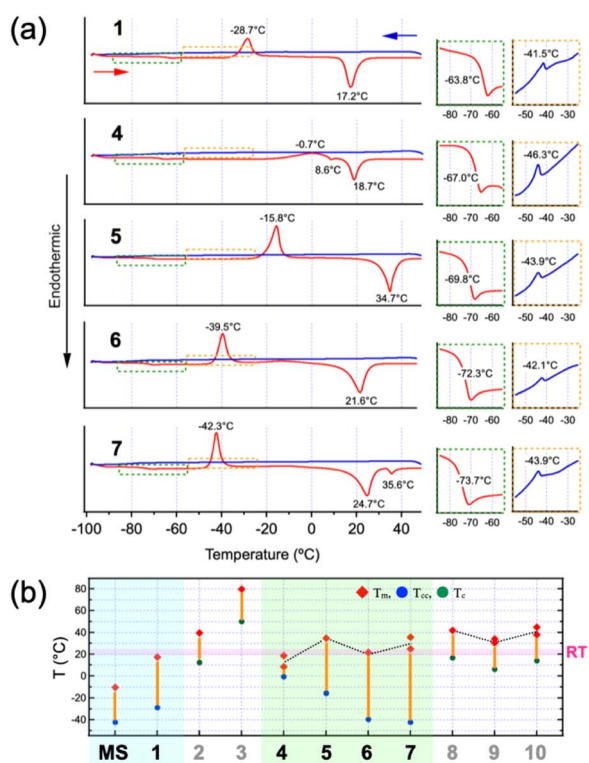


Fig. 2 (a) DSC thermograms of liquid samples (**1**, **4**, **5**, **6**, and **7**). All samples were first heated from RT to  $50\text{ }^{\circ}\text{C}$ , and then subjected to cooling and reheating at a rate of  $10\text{ }^{\circ}\text{C min}^{-1}$ . The cooling and heating processes are represented by blue and red lines, respectively. The regions with weak signals (highlighted by green and orange dotted lines) are enlarged and displayed on the right side. (b) Graphical representation of the thermal data presented in Table S1, SI.

recognized as another key phenomenon in the thermal phase transitions of small molecules.<sup>47–51</sup> Among the molecules exhibiting CC reported so far, the MS-based liquid is, to our knowledge, the smallest, comparable in size to the imidazolium-based ionic liquids.<sup>52</sup> The CC behaviour observed in the MS liquids is likely not explained solely by van der Waals (vdW) interactions between the alkoxy chains, since alkanes such as butane, pentane, hexane, and heptane all exhibit much lower freezing points (below approximately  $-100\text{ }^{\circ}\text{C}$ ). Thus, the occurrence of CC implies that the MS  $\pi$ -moiety has a tendency to aggregate, even though it possesses only a small  $\pi$ -system and lacks coulombic interactions typically observed in the imidazolium-based ionic liquids. Based on the CC temperatures ( $T_{cc}$ ) of the yellow liquids, their crystallizability increases with alkoxy chain length ( $7 > 6 > 5 > 4$ ), suggesting that alkoxy chain interactions may support crystallization alongside the primary stacking of the MS  $\pi$ -moieties. Notably, even MS itself exhibits CC (Fig. S7, SI). However, the stacking structures of MS and **1**, both of which are colourless liquids, must differ from those of the yellow liquids (**4–7**). This suggests that the aggregates responsible for the yellow coloration are not efficiently formed if alkoxy chain interactions are absent. On the other hand, their  $T_m$  values, which are close to room temperature (RT), show a slight indication of an odd–even effect (Fig. 2b). As an



additional note, the appearance of two  $T_m$  peaks in **4** and **7** may suggest a possibility that their crystalline states are polymorphic.

### X-ray diffraction analysis of MS liquids

To confirm the presence of microscopic local  $\pi$ -aggregate structures within the macroscopically homogeneous liquid phase, X-ray diffraction (XRD) measurements were carried out. As a result, two halos were detected (Fig. 3a). The left-side halos shift to lower  $q$  values as the alkoxy chain length increases, whereas the right-side halos appear around  $q \approx 1.5 \text{ \AA}^{-1}$ , irrespective of the chain length. In fact, alkyl- $\pi$  molecular liquids often exhibit similar XRD profiles with two such halos: one originating from molten aliphatic chains, and the other from the averaged distance between  $\pi$  units.<sup>9,25,53-55</sup> Compared to these alkyl- $\pi$  molecules, however, our MS molecules are much more compact in size, both in their  $\pi$  and chain moieties, and not bulky. For this reason, similar attributions would not be suitable. The  $d$ -spacing of  $4.0\text{--}4.3 \text{ \AA}$ , obtained from  $q \approx 1.5 \text{ \AA}^{-1}$ , is approximately in agreement with that of the benzene dimer in the offset parallel stacking mode, as determined from neutron diffraction results for liquid benzene.<sup>56,57</sup> We previously reported the tentative model of the MS aggregates using methyl 5-methoxysalicylate (*i.e.*, **1**) molecules, where they adopt a slipped antiparallel stacking arrangement. In this model (Fig. 3b), the interplanar distance is  $3.3 \text{ \AA}$ , and the center-to-center distance between the aromatic rings is  $5.4 \text{ \AA}$ . Considering that, on the time scale of XRD measurements, the molecules are sufficiently dynamic and are not fixed in static local structures, it is reasonable to assume that this dimeric configuration could give rise to a diffraction halo corresponding to a  $d$ -spacing of approximately  $4.2 \text{ \AA}$ . On the other hand, the left-side halos, which shift depending on the chain length, give much larger  $d$ -spacing values. Since it is impossible to assume these large distances using an MS molecule with a single benzene ring,  $\pi$ -aggregates involving more than a dimer must be considered.

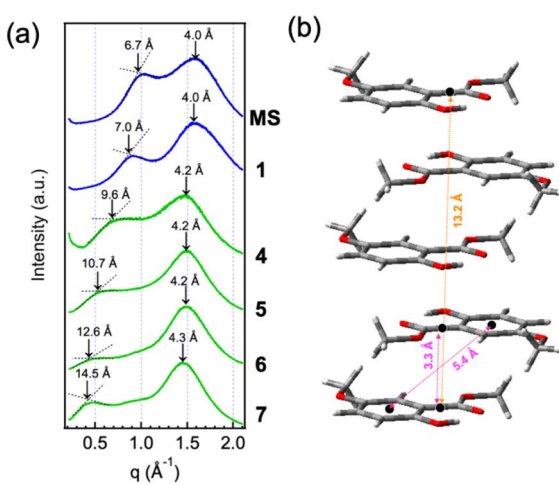


Fig. 3 (a) XRD patterns of liquid samples (MS, **1**, **4**, **5**, **6**, and **7**) at RT. (b) The pentamer model for MS aggregates in the liquid state, constructed using five molecules of **1** as described in ref. 14.

Based on the combined interplanar distances in the aggregation model,  $\pi$ -aggregates ranging from trimers to pentamers could exist within the macroscopically homogeneous liquid phase. In addition, elongation of the alkoxy chain appears to promote aggregate growth, enabling the formation of larger aggregates. It is experimentally difficult to determine the molecular arrangement within aggregates in the neat liquid state. Therefore, molecular dynamics (MD) simulations remain a future challenge for us.

### Liquid physical properties related to molecular mobility

Although the viscosity of the MS liquids was not experimentally measured, it is presumed to be low and comparable to that of common organic solvents, as suggested by its flow behaviour during handling (see Movie S1, SI). Such fluidity appears reasonable, given the small and simple structure of the MS molecules and their weak intermolecular interactions. With regard to density ( $\rho$ ), there is a distinct discontinuity between the colourless liquids (MS and **1**) and the yellow liquids (**4**–**7**), and a gradual decrease is observed as the alkoxy chain length increases from **4** to **7** (Fig. 4a). On the other hand, free volume is a key parameter for understanding molecular mobility and viscosity, and was therefore also evaluated using positron annihilation lifetime spectroscopy (PALS) (Fig. S8 and Table S2, SI). In this technique, the longest-lived component of the positron lifetime spectrum ( $\tau_3$ ) is attributed to *ortho*-positronium annihilation in intermolecular free-volume regions, and its intensity ( $I_3$ ) reflects the relative amount of such free volume.<sup>54</sup> In the present system, the  $\tau_3$  values are approximately in the range of 2.5 to 2.7 ns, irrespective of chain length (Fig. 4b, red markers). Based on the Tao-Eldrup model,<sup>58,59</sup> which approximates the free-volume holes as spheres, the mean hole radius can be estimated from  $\tau_3$ , corresponding to a hole volume ( $V_h$ ) in the range of 140 to 170  $\text{\AA}^3$  (Fig. 4c). Although this model provides a static estimate of free volume, the values could be used as a structural parameter to discuss trends in dynamic free volume in soft matter systems.<sup>60</sup> The larger  $V_h$  observed in the yellow liquids (**4**–**7**), compared to the colourless liquids (MS and **1**), may be due to the fact that longer alkoxy chains make molecular packing less efficient, resulting in larger

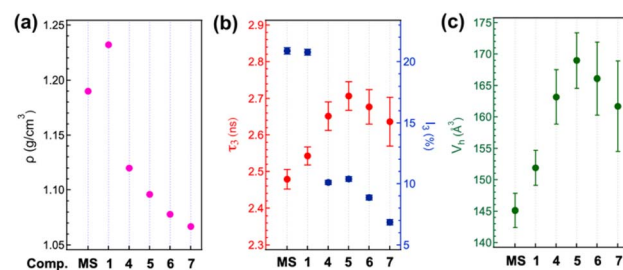


Fig. 4 Density and free volume of the MS-based RT liquids plotted against chain length: (a) density ( $\rho$ ); (b)  $\tau_3$  and  $I_3$  values, represented by red and blue markers, respectively, and obtained from positron annihilation lifetime spectroscopy (PALS); (c) hole volume ( $V_h$ ) estimated from  $\tau_3$  using Tao-Eldrup model. See Table S2 for details of the data and calculations.



free volume. However, when comparing among the yellow liquids (4–7), the gradual decrease in  $V_h$  with increasing chain length may suggest that longer chains allow for more efficient molecular packing, *i.e.*, the formation of  $\pi$ -aggregates; such an interpretation is also consistent with the DSC and XRD results mentioned above. On the other hand, it should be noted that the  $I_3$  value for the yellow liquids is markedly lower (approximately 10% or less), indicating fewer free-volume regions—less than half of that observed for the colourless liquids (Fig. 4b, blue makers). This further supports the interpretation that the MS moieties in the yellow liquids are closely stacked, aided by the vdW interactions between the alkoxy chains.

### Fluorescence lifetime measurement of the MS samples

To verify that the characteristic fluorescence of the MS liquid arises from the formation of supramolecular  $\pi$ -aggregates, time-resolved fluorescence spectroscopy measurements were conducted (Fig. 5a: representative sample results; Table S3, SI: analytical data for all samples; Fig. 5b: visual representation corresponding to Table S3). Regardless of whether the sample is a powder (*e.g.*, 2 and 9) or a liquid (*e.g.*, 1 and 5), their dilute solutions exhibited identical fluorescence spectra (Fig. S1, SI) and nearly overlapping fluorescence decay curves, with a lifetime ( $\tau$ ) of 0.5 ns (Fig. 5a, blue plots), although additional components with  $\tau$  values approximately an order of magnitude longer were moderately observed in samples 8, 9, and 10 (Fig. 5b, top).

On the other hand, the decay curves for the neat samples are significantly broader than those for their dilute solutions (Fig. 5a, grey and green plots). In particular, this broadening is noticeable in the liquid samples of 1 and 5, for which exponential fittings indicate the presence of two components: a fast

$\tau_1$  of a few ns and a slower  $\tau_2$  of approximately 20 ns (Fig. 5b, bottom). In 1, the slower  $\tau_2$  component accounts for nearly 90% of the total emission, indicating that most of the excitation energy is received by  $\pi$ -aggregates that are too unstable to exhibit the characteristic fluorescence observed in the yellow liquids (4–7). The dominant  $\tau_2$  component thus likely originates from these weakly bound  $\pi$ -aggregates. In contrast, in the yellow liquids, the  $\tau_2$  components constitute 30–50% of the total emission, increasing with chain elongation. Since the  $\pi$ -aggregates in the yellow liquids are not effectively excited at the excitation wavelength  $\lambda_{\text{ex}} = 375$  nm as their absorption band is located in the 400–500 nm region, it is plausible that the fluorescence observed at  $\lambda_{\text{em}} = 500$  nm is caused by energy transfer from monomers (faster  $\tau_1$  component) to the  $\pi$ -aggregates (slower  $\tau_2$  component). Considering this, the presence of these two  $\tau$  components clearly demonstrates the coexistence of monomers and  $\pi$ -aggregates in the yellow liquids. It is likely that, on the timescale of fluorescence, the  $\pi$ -aggregates in 4–7 are tightly bound enough to enable delocalized excitation over multiple molecules, giving rise to their characteristic optical properties. Furthermore, it is evident that such  $\pi$ -aggregates, associated with the slower  $\tau_2$  component, are not present in the yellow powder samples 8–10.

### Enhanced $\pi$ -aggregate formation in the melted state

According to the DSC results (Fig. 2b), all powders except for 3 melted at relatively low temperatures below 50 °C and formed a liquid phase. These liquids became capable of exhibiting light green fluorescence, similar to that of the RT liquids of 4–7. Notably, even 2 and 3, which were originally blue fluorescent powders, turned into light green fluorescent liquids upon melting (Fig. 6a). For both 2 and 8, although the fluorescence intensities decreased markedly upon heating, the melted states

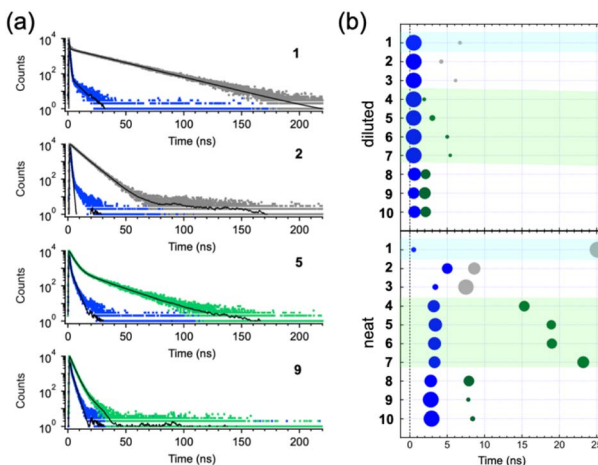


Fig. 5 (a) Time-resolved fluorescence decay curves of liquid samples 1 and 5, and powder samples 2 and 9. Blue traces correspond to diluted samples (3 × 10<sup>-4</sup> M in chloroform;  $\lambda_{\text{ex}} = 375$  nm,  $\lambda_{\text{em}} = 400$  nm). Grey and green traces represent neat samples ( $\lambda_{\text{ex}} = 375$  nm,  $\lambda_{\text{em}} = 450$  nm for 1; 400 nm for 2 and 3; 500 nm for 4–10). (b) Visual representation of the numerical data presented in Table S3, SI. Blue and green circles indicate the short- and long-lifetime components, respectively, with circle size reflecting their relative contributions.

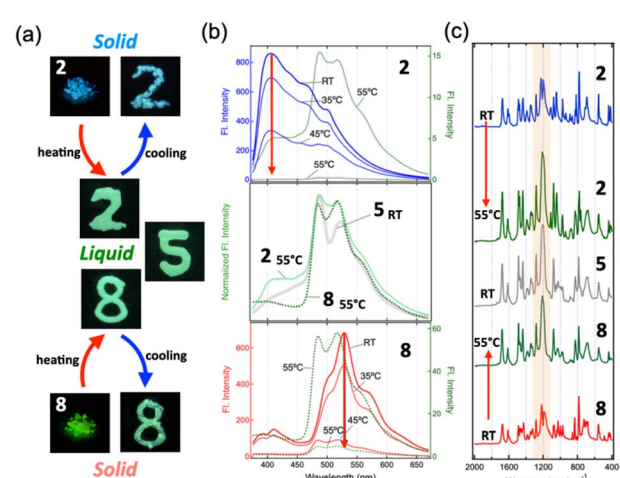


Fig. 6 (a) Photographs of 2 and 8 under 365 nm UV irradiation: before and after heating at 55 °C, and after cooling, along with the RT liquid 5. (b) Fluorescence spectral changes of 2 (top) and 8 (bottom) upon heating. The middle panel shows a spectral comparison of 2 and 8 at 55 °C with 5. (c) IR spectral changes of 2 and 8 upon heating to 55 °C, compared with the spectrum of 5 at RT. IR spectra of the other samples at RT are provided in Fig. S9, SI.



exhibited the same fluorescence spectra as the RT liquid of **5**, in which the two vibronic peaks at 487 nm ( $20\,533\text{ cm}^{-1}$ ) and 518 nm ( $19\,305\text{ cm}^{-1}$ ) exactly matched (Fig. 6b, mid panel). This indicates that the fluidity caused by melting promotes the formation of  $\pi$ -aggregates, which appears to be identical to those present in the RT liquids. In contrast, the crystalline phase of the RT liquid **4**, obtained by cold crystallization near  $0\text{ }^\circ\text{C}$ , exhibited a fluorescence spectrum almost identical to that of **8** (Fig. S10, SI). Therefore,  $\pi$ -aggregates are observed exclusively in the liquid state.

The  $\pi$ -aggregate formation resulting from heating and dissolving the powder samples induces a distinct IR spectral change, with the signal around  $1200\text{ cm}^{-1}$  being significantly enhanced (Fig. 6c). We previously investigated the origin of the fine vibronic progression observed in the absorption and fluorescence spectra of MS-dyads by carrying out a normal-mode analysis of the  $\pi$ -aggregate model shown in Fig. 3b.<sup>14</sup> The results suggested that association of the MS molecules activates a vibrational mode mainly characterized by the C–O stretching of the methylcarboxyl group, which evolves into a collective motion involving all constituent MS molecules of the  $\pi$ -aggregate. We thus concluded that such a collective mode is strongly coupled with the electronic transition of the  $\pi$ -aggregate, thereby giving rise to the fine vibronic progression of the spectra. When this interpretation is applied to the present system, the energy of the association-induced collective mode is about  $1200\text{ cm}^{-1}$ , which is in reasonable agreement with the energy difference between the two vibronic peaks ( $1228\text{ cm}^{-1}$ ). Therefore, the IR measurements of the neat sample in this work successfully captured the vibrational states before and after aggregation; as a result, our interpretation of the origin of the vibronic progression was experimentally verified.

Moreover, XRD measurements were performed on the heated sample to detect possible  $\pi$ -aggregates in the melted state. The sample of **9** was measured immediately after heating and melting. Although crystallization progressed over time as the sample cooled down resulting in several sharp peaks, a halo with a *d*-spacing of  $19.3\text{ \AA}$ , larger than that of **7** shown in Fig. 3a, was also observed (Fig. S11, SI). The above results demonstrate that MS tends to form  $\pi$ -aggregates only in the condensed liquid phase when its alkoxy chain contains two or more carbon atoms, and that the extent of aggregate growth increases with the alkoxy chain length.

## Conclusions

In conclusion, we demonstrated that alkoxylation of methyl salicylate (MS) at the 5-position induces the formation of supramolecular  $\pi$ -aggregates in the liquid state, significantly altering its optical properties. The transformation to a vivid yellow liquid with distinct absorption and fluorescence features was observed for derivatives bearing alkoxy chains of four or more carbon atoms (**4**–**7**), suggesting extended  $\pi$ -electron delocalization across multiple MS units. Structural characterization based on XRD measurements confirmed the presence of  $\pi$ -aggregates with dimensions of  $10$ – $15\text{ \AA}$ , involving three to five MS molecules arranged *via* face-to-face  $\pi$ -stacking. Supporting

this aggregation behaviour, DSC measurements suggested that cold crystallization originates from  $\pi$ -aggregation under high-density conditions, despite the small and simple molecular structure. PALS measurements further suggested that the yellow liquids (**4**–**7**) are in a more densely packed state compared to the colourless liquids (MS and **1**). In addition, fluorescence lifetime measurement of **4**–**7** revealed a long-lived emission component arising from energy transfer from the monomeric state to the  $\pi$ -aggregated state. These results provide direct evidence that even relatively simple and small molecules can lead to microscopic local structural aggregates in liquids, with substantial influence on macroscopic properties such as colour and fluorescence. These results provide direct evidence that even relatively simple and small molecules can lead to microscopic local structural aggregates in liquids, with substantial influence on macroscopic properties such as colour and fluorescence. Only weak intermolecular interactions—such as dipole–dipole and dispersion forces between the small  $\pi$ -systems of the constituent MS molecules—are present within these aggregates. This is in contrast to ionic liquids, where structural heterogeneity is formed by the distinct coulombic attraction between the positively and negatively charged components, as well as by the possible formation of hydrogen-bonding networks.<sup>35</sup> Nevertheless,  $\pi$ -aggregates with delocalized  $\pi$ -electrons across multiple molecules may form due to several factors, including (1) the realization of a condensed state unique to liquids, (2) compatibility of intermolecular orbital mixing,<sup>14</sup> and (3) the presence of alkyl chains of appropriate length that stabilize the  $\pi$ -stacking structure. Following these design principles, we have tentatively identified additional potential candidates besides the MS liquids. The present study demonstrates that the condensed state of liquids uniquely enables the formation of  $\pi$ -aggregates capable of generating new electronic states, offering a promising platform for the development of advanced optical and electronic functionalities.

## Author contributions

K. K. carried out a series of measurements. K. S. conceived and supervised the project and wrote the manuscript. T. A. and T. N. also supervised the project.

## Conflicts of interest

There are no conflicts to declare.

## Data availability

All data supporting the findings of this study are included within the article and its supplementary information (SI) files. Supplementary information: experimental details, synthetic procedures, and additional data such as optical, DSC, PALS, fluorescence lifetime, ATR-IR, and XRD measurements (Fig. S1–S11 and Tables S1–S3). See DOI: <https://doi.org/10.1039/d5sc06148b>.



## Acknowledgements

This work was supported by the NIMS Joint Research Hub Program (2024-49), a research grant from the Takahashi Industrial and Economic Research Foundation, and was partially supported by a Grant-in-Aid for Scientific Research (KAKENHI, Grant No. 25K0870, Category C) from the Ministry of Education, Culture, Sports, Science and Technology (MEXT). Part of this work was also conducted under the research program “Dynamic Alliance for Open Innovation Bridging Human, Environment and Materials” in the “Network Joint Research Center for Materials and Devices.” We thank Dr Akito Tateyama for his kind assistance in several measurements at NIMS.

## Notes and references

- 1 M. D. Curtis, J. Cao and J. W. Kampf, Solid-State Packing of Conjugated Oligomers: From  $\pi$ -Stacks to the Herringbone Structure, *J. Am. Chem. Soc.*, 2004, **126**, 4318–4328.
- 2 S. Inoue, H. Minemawari, J. Y. Tsutsumi, M. Chikamatsu, T. Yamada, S. Horiuchi, M. Tanaka, R. Kumai, M. Yoneya and T. Hasegawa, Effects of Substituted Alkyl Chain Length on Solution-Processable Layered Organic Semiconductor Crystals, *Chem. Mater.*, 2015, **27**, 3809–3812.
- 3 J.-C. Ribierre, Z. Li, X. Liu, E. Lacaze, B. Heinrich, S. Méry, P. Słęczkowski, Y. Xiao, F. Lafolet, D. Hashizume, T. Aoyama, M. Uchiyama, J. W. Wu, E. Zaborova, F. Fages, A. D’Aléo, F. Mathevet and C. Adachi, A solvent-free and vacuum-free melt-processing method to fabricate organic semiconducting layers with large crystal size for organic electronic applications, *J. Mater. Chem. C*, 2019, **7**, 3190–3198.
- 4 E. T. Samulski, M. M. Gauthier, R. B. Blumstein and A. Blumstein, Alkyl chain order in a linear polymeric liquid crystal, *Macromolecules*, 1984, **17**, 479–483.
- 5 S. Santhosh Babu and T. Nakanishi, Nonvolatile functional molecular liquids, *Chem. Commun.*, 2013, **49**, 9373–9382.
- 6 A. Ghosh and T. Nakanishi, Frontiers of solvent-free functional molecular liquids, *Chem. Commun.*, 2017, **53**, 10344–10357.
- 7 T. Machida and T. Nakanishi, Alkyl- $\pi$  functional molecular liquids towards soft electronics, *J. Mater. Chem. C*, 2021, **9**, 10661–10667.
- 8 B. A. Kamino, T. P. Bender and R. A. Klenkler, Hole Mobility of a Liquid Organic Semiconductor, *J. Phys. Chem. Lett.*, 2012, **3**, 1002–1006.
- 9 A. Ghosh, M. Yoshida, K. Suemori, H. Isago, N. Kobayashi, Y. Mizutani, Y. Kurashige, I. Kawamura, M. Nirei, O. Yamamoto, T. Takaya, K. Iwata, A. Saeki, K. Nagura, S. Ishihara and T. Nakanishi, Soft chromophore featured liquid porphyrins and their utilization toward liquid electret applications, *Nat. Commun.*, 2019, **10**, 4210.
- 10 S. Hotta and T. Yamao, The thiophene/phenylene co-oligomers: exotic molecular semiconductors integrating high-performance electronic and optical functionalities, *J. Mater. Chem.*, 2011, **21**, 1295–1304.
- 11 Y. Hong, J. W. Y. Lam and B. Z. Tang, Aggregation-induced emission, *Chem. Soc. Rev.*, 2011, **40**, 5361–5388.
- 12 F. Würthner, T. E. Kaiser and C. R. Saha-Moeller, J-Aggregates: From Serendipitous Discovery to Supramolecular Engineering of Functional Dye Materials, *Angew. Chem., Int. Ed.*, 2011, **50**, 3376–3410.
- 13 S. Hayashi, Cyano-substituted oligo(*p*-phenylene-vinylene)s having linear and branched octyloxy groups: control of aggregation and emission properties via C8 alkyl chain difference, *Mol. Syst. Des. Eng.*, 2021, **6**, 503–507.
- 14 M. Takahashi, K. Sakai, K. Sambe and T. Akutagawa, Supramolecular Complexation and Collective Optical Properties Induced by Linking Two Methyl Salicylates via a  $\sigma$ -Bridge, *J. Phys. Chem. B*, 2022, **126**, 3116–3124.
- 15 K. Kobayashi, K. Sakai, S. Suzuki, Y. Imai, T. Tsushima and T. Akutagawa, Supramolecular Chirality Achieved by Assembly of Small  $\pi$ -Molecules of Octahydrobinaphthols with Axial Chirality, *J. Phys. Chem. B*, 2024, **128**, 4464–4471.
- 16 S. Grimme, Do Special Noncovalent  $\pi$ - $\pi$  Stacking Interactions Really Exist?, *Angew. Chem., Int. Ed.*, 2008, **47**, 3430–3434.
- 17 C. R. Martinez and B. L. Iverson, Rethinking the term “pi-stacking”, *Chem. Sci.*, 2012, **3**, 2191–2201.
- 18 K. Carter-Fenk and J. M. Herbert, Reinterpreting  $\pi$ -stacking, *Phys. Chem. Chem. Phys.*, 2020, **22**, 24870–24886.
- 19 S. Santhosh Babu, J. Aimi, H. Ozawa, N. Shirahata, A. Saeki, S. Seki, A. Ajayaghosh, H. Möhwald and T. Nakanishi, Solvent-Free Luminescent Organic Liquids, *Angew. Chem., Int. Ed.*, 2012, **51**, 3391–3395.
- 20 T. Machida, R. Taniguchi, T. Oura, K. Sada and K. Kokado, Liquefaction-induced emission enhancement of tetraphenylethene derivatives, *Chem. Commun.*, 2017, **53**, 2378–2381.
- 21 Goudappagouda, A. Manthanath, V. C. Wakchaure, K. C. Ranjeesh, T. Das, K. Vanka, T. Nakanishi and S. S. Babu, Paintable Room-Temperature Phosphorescent Liquid Formulations of Alkylated Bromonaphthalimide, *Angew. Chem., Int. Ed.*, 2019, **58**, 2284–2288.
- 22 K. Isoda, T. Ishiyama, Y. Mutoh and D. Matsukuma, Stimuli-Responsive Room-Temperature N-Heteroacene Liquid: *In Situ* Observation of the Self-Assembling Process and Its Multiple Properties, *ACS Appl. Mater. Interfaces*, 2019, **11**, 12053–12062.
- 23 F. Lu, K. Hagiwara, M. Yoshizawa, K. Nagura, S. Ishihara and T. Nakanishi, Luminescence tuning with excellent colour homogeneity and steadiness using fluorescent molecular liquids, *J. Mater. Chem. C*, 2019, **7**, 2577–2582.
- 24 F. Lu and T. Nakanishi, Solvent-Free Luminous Molecular Liquids, *Adv. Opt. Mater.*, 2019, **7**, 1900176.
- 25 X. Bai, Y. Sun, Y. Jiang, G. Zhao, J. Jiang, C. Yuan and M. Liu, Circularly Polarized Luminescence from Solvent-Free Chiral Organic  $\pi$ -Liquids, *Angew. Chem., Int. Ed.*, 2021, **60**, 3745–3751.
- 26 A. Ikenaga, Y. Akiyama, T. Ishiyama, M. Gon, K. Tanaka, Y. Chujo and K. Isoda, Stimuli-Responsive Self-Assembly of  $\pi$ -Conjugated Liquids Triggers Circularly Polarized



Luminescence, *ACS Appl. Mater. Interfaces*, 2021, **13**, 47127–47133.

27 K. Takaishi, T. Matsumoto, M. Kawata and T. Ema, Circularly Polarized Luminescence Liquids Based on Siloxybinaphthyls: Best Binaphthyl Dihedral Angle in the Excited State, *Angew. Chem., Int. Ed.*, 2021, **60**, 9968–9972.

28 X. Wen, S. Du, L. Zhang and M. Liu, Chiral Deep Eutectic Solvents Enable Full-Color and White Circularly Polarized Luminescence from Achiral Luminophores, *Angew. Chem., Int. Ed.*, 2023, **62**, e202311816.

29 Z. Xiao, R. Wang, L. Zhang and M. Liu, A fluorinated chiral liquid with thermal robustness for inducing circularly polarized luminescence, *Chem. Commun.*, 2025, **61**, 764–767.

30 K. Kushwaha, L. Yu, K. Stranius, S. K. Singh, S. Hultmark, M. N. Iqbal, L. Eriksson, E. Johnston, P. Erhart, C. Müller and K. Börjesson, A Record Chromophore Density in High-Entropy Liquids of Two Low-Melting Perylenes: A New Strategy for Liquid Chromophores, *Adv. Sci.*, 2019, **6**, 1801650.

31 A. Ghoufi, Molecular Origin of the Prepeak in the Structure Factor of Alcohols, *J. Phys. Chem. B*, 2020, **124**, 11501–11509.

32 A. Mariani, A. Innocenti, A. Varzi and S. Passerini, On the nanoscopic structural heterogeneity of liquid *n*-alkyl carboxylic acids, *Phys. Chem. Chem. Phys.*, 2021, **23**, 20282–20287.

33 J. Grelska, K. Jurkiewicz, A. Burian and S. Pawlus, Supramolecular Structure of Phenyl Derivatives of Butanol Isomers, *J. Phys. Chem. B*, 2022, **126**, 3563–3571.

34 J. Grelska, K. Jurkiewicz, A. Nowok and S. Pawlus, Computer simulations as an effective way to distinguish supramolecular nanostructure in cyclic and phenyl alcohols, *Phys. Rev. E*, 2023, **108**, 024603.

35 R. Hayes, G. G. Warr and R. Atkin, Structure and Nanostructure in Ionic Liquids, *Chem. Rev.*, 2015, **115**, 6357–6426.

36 X. Zheng, K. Nagura, T. Takaya, K. Hashi and T. Nakanishi, Quest for a Rational Molecular Design of Alkyl-Distyrylbenzene Liquid by Substitution Pattern Modulation, *Chem.-Eur. J.*, 2023, **29**, e202203775.

37 Y. Yamamoto, F. Lu, T. Nakanishi and S. Hayashi, Liquid Structures and Diffusion Dynamics of Alkyl-Pyrene Liquids Studied by Molecular Dynamics Simulations, *J. Phys. Chem. B*, 2023, **127**, 4870–4885.

38 Z. Guo, C. Pan, A. Shinohara and T. Nakanishi, Merging  $\pi$ -molecular functions achieved through homogeneous liquid-liquid blending of solvent-free alkyl- $\pi$  liquids, *Sci. Technol. Adv. Mater.*, 2025, **26**, 2515007.

39 A. U. Acuna, F. Amat-Guerri, J. Catalan and F. Gonzalez-Tablas, Dual fluorescence and ground state equilibria in methyl salicylate, methyl 3-chlorosalicylate, and methyl 3-*tert*-butylsalicylate, *J. Phys. Chem.*, 1980, **84**, 629–631.

40 Y. Li, Y. Ma, Y. Yang, W. Shi, R. Lan and Q. Guo, Effects of different substituents of methyl 5-R-salicylates on the excited state intramolecular proton transfer process, *Phys. Chem. Chem. Phys.*, 2018, **20**, 4208–4215.

41 B. Wunderlich, Theory of Cold Crystallization of High Polymers, *J. Chem. Phys.*, 1958, **29**, 1395–1404.

42 S. Sampath, A. A. Boopathi and A. B. Mandal, “Bottom-up” self-assembly and “cold crystallization” of butterfly shaped tetrabenzo[fluorene molecules, *Phys. Chem. Chem. Phys.*, 2016, **18**, 21251–21258.

43 Y. Tsujimoto, T. Sakurai, Y. Ono, S. Nagano and S. Seki, Cold Crystallization of Ferrocene-Hinged  $\pi$ -Conjugated Molecule Induced by the Limited Conformational Freedom of Ferrocene, *J. Phys. Chem. B*, 2019, **123**, 8325–8332.

44 A. Honda, S. Kakihara, M. Kawai, T. Takahashi and K. Miyamura, Cold Crystallization and Polymorphism Triggered by the Mobility of the Phenyl Group in Alkyl Azo Dye Molecules, *Cryst. Growth Des.*, 2021, **21**, 6223–6229.

45 K. Ishino, H. Shingai, Y. Hikita, I. Yoshikawa, H. Houjou and K. Iwase, Cold Crystallization and the Molecular Structure of Imidazolium-Based Ionic Liquid Crystals with a p-Nitroazobenzene Moiety, *ACS Omega*, 2021, **6**, 32869–32878.

46 K. Iwase, Y. Toyama, I. Yoshikawa, Y. Yamamura, K. Saito and H. Houjou, Insight into Structural Demand for Cold Crystallization of a Small Molecule. A Case Study for Schiff Base Compounds that Exhibit Prototropic Tautomerization, *Bull. Chem. Soc. Jpn.*, 2018, **91**, 669–677.

47 Y. Sun, H. Xi, S. Chen, M. D. Ediger and L. Yu, Crystallization near Glass Transition: Transition from Diffusion-Controlled to Diffusionless Crystal Growth Studied with Seven Polymorphs, *J. Phys. Chem. B*, 2008, **112**, 5594–5601.

48 R. J. Greet and D. Turnbull, Glass Transition in *o*-Terphenyl, *J. Chem. Phys.*, 1967, **46**, 1243–1251.

49 T. Hikima, Y. Adachi, M. Hanaya and M. Oguni, Determination of potentially homogeneous-nucleation-based crystallization in *o*-terphenyl and an interpretation of the nucleation-enhancement mechanism, *Phys. Rev. B: Condens. Matter Mater. Phys.*, 1995, **52**, 3900–3908.

50 D. Musumeci, C. T. Powell, M. D. Ediger and L. Yu, Termination of Solid-State Crystal Growth in Molecular Glasses by Fluidity, *J. Phys. Chem. Lett.*, 2014, **5**, 1705–1710.

51 K. Paeng and L. J. Kaufman, Which probes can report intrinsic dynamic heterogeneity of a glass forming liquid?, *J. Chem. Phys.*, 2018, **149**, 164501.

52 T. Endo, T. Kato, K.-I. Tozaki and K. Nishikawa, Phase Behaviors of Room Temperature Ionic Liquid Linked with Cation Conformational Changes: 1-Butyl-3-Methylimidazolium Hexafluorophosphate, *J. Phys. Chem. B*, 2010, **114**, 407–411.

53 F. Lu, T. Takaya, K. Iwata, I. Kawamura, A. Saeki, M. Ishii, K. Nagura and T. Nakanishi, A Guide to Design Functional Molecular Liquids with Tailorable Properties using Pyrene-Fluorescence as a Probe, *Sci. Rep.*, 2017, **7**, 3416.

54 B. Narayan, K. Nagura, T. Takaya, K. Iwata, A. Shinohara, H. Shinmori, H. Wang, Q. Li, X. Sun, H. Li, S. Ishihara and T. Nakanishi, The effect of regiosomerism on the photophysical properties of alkylated-naphthalene liquids, *Phys. Chem. Chem. Phys.*, 2018, **20**, 2970–2975.

55 F. Lu, K. Jang, I. Osica, K. Hagiwara, M. Yoshizawa, M. Ishii, Y. Chino, K. Ohta, K. Ludwichowska, K. J. Kurzydłowski, S. Ishihara and T. Nakanishi, Supercooling of functional alkyl- $\pi$  molecular liquids, *Chem. Sci.*, 2018, **9**, 6774–6778.



56 T. F. Headen, Temperature dependent structural changes in liquid benzene studied using neutron diffraction, *Mol. Phys.*, 2019, **117**, 3329–3336.

57 T. F. Headen, C. A. Howard, N. T. Skipper, M. A. Wilkinson, D. T. Bowron and A. K. Soper, Structure of  $\pi$ – $\pi$  Interactions in Aromatic Liquids, *J. Am. Chem. Soc.*, 2010, **132**, 5735–5742.

58 S. J. Tao, Positronium Annihilation in Molecular Substances, *J. Chem. Phys.*, 1972, **56**, 5499–5510.

59 M. Eldrup, D. Lightbody and J. N. Sherwood, The temperature dependence of positron lifetimes in solid pivalic acid, *Chem. Phys.*, 1981, **63**, 51–58.

60 N. J. Brooks, F. Castiglione, C. M. Doherty, A. Dolan, A. J. Hill, P. A. Hunt, R. P. Matthews, M. Mauri, A. Mele, R. Simonutti, I. J. Villar-Garcia, C. C. Weber and T. Welton, Linking the structures, free volumes, and properties of ionic liquid mixtures, *Chem. Sci.*, 2017, **8**, 6359–6374.

